Dynamic laser beam shaping for material processing using hybrid holograms

Dun Liu[1,2]， Yutao Wang[2], Zhongsheng Zhai[1,2*], , Zheng Fang[2], Qing Tao[1,2], Walter Perrie[3], Stuart P Edwardson[3], and Geoff Dearden[3]

1 Hubei Key Laboratory of Modern Manufacturing Quantity Engineering，School of Mechanical Engineering, Hubei University of Technology, Wuhan, China

2 Laser Group, School of Mechanical Engineering, Hubei University of Technology, Wuhan, China

3 Laser Group, Department of Engineering, University of Liverpool, Brownlow street, Liverpool, L69 3GQ, UK

[*]Corresponding authors: zs.zhai@hbut.edu.cn

Graphical abstract

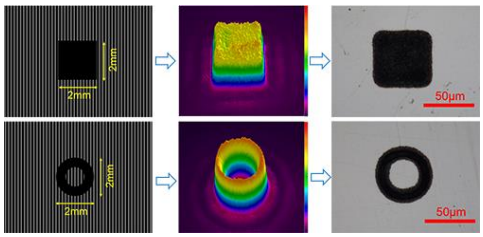

Research highlights

High quality arbitrary beam profile with low edge diffraction effect can be obtained.

The shaped beam can be reconstructed in the range of 0.5 mm at the image plane.

The beam local energy ratio observed by the CCD camera is up to 77.67%.

Dynamic beam shaping with a refresh rate of 25 Hz has been achieved.

Abstract

A high quality, dynamic laser beam shaping method is demonstrated by displaying a series of hybrid holograms onto a spatial light modulator (SLM), while each one of the holograms consists of a binary grating and a geometric mask. A

diffraction effect around the shaped beam has been significantly reduced. Beam profiles of arbitrary shape, such as square, ring, triangle, pentagon and hexagon, can be conveniently obtained by loading the corresponding holograms on the SLM. The shaped beam can be reconstructed in the range of 0.5 mm at the image plane. Ablation on a polished stainless steel sample at the image plane are consistent with the beam shape at the diffraction near-field. The ±1st order and higher order beams can be completely removed when the grating period is smaller than 160μm. The local energy ratio of the shaped beam observed by the CCD camera is up to 77.67%. Dynamic processing at 25 Hz using different shapes has also been achieved.

Keywords: beam shaping; binary grating; geometric mask; spatial light modulator

1. Introduction

For high precision laser machining, sometimes shaped beams have advantages comparing to a Gaussian beam [1-4]. Spatial light modulator (SLM), as a programmable diffractive optical device, can dynamically adjust the properties of an incident beam [5-7]. Some researchers used the SLM to transform a incident Gaussian beam into different shapes for micro-manipulation [8-10]. Sanner et al. obtained top-hat, doughnut, square, and triangle beam shapes at the focal plane using a non-pixelated optically addressed light valve [11]. Kuang et al. successfully obtained similar shaped beams at the image plane using geometric masks with an SLM [12], but the steep grayscale change at the edge of the masks results in a severe edge diffraction effect. In order to produce high quality shaped beams with accuracy, flexibility and speed, imaging-based phase and amplitude modulation has also been demonstrated [13-16].

In this paper, a dynamic laser beam shaping method is presented using hybrid holograms, which are combined by binary gratings and geometric masks. The edge diffraction effect has been significantly reduced. Top-hat beams with arbitrary profile, such as square, ring, triangle, pentagon and hexagon, can be obtained in the diffraction near-field by loading corresponding holograms onto the SLM. The shaped beam can be reconstructed in a range near the image plane. The local energy ratio of the shaped beam observed by the CCD camera is up to 77.67%. Dynamic machining with shaped beams at 25Hz on a polished stainless steel sample is also demonstrated.

2. Experiment and methodology

2.1 Experimental setup

Fig. 1 shows the schematic of the experimental setup. The laser beam with a 9 mm diameter from a femtosecond laser amplifier (Libra-HE, with 800 nm central wavelength, 100fs pulse width, 400μJ pulse energy and 10kHz repetition rate) passed

through an attenuator, a shutter and a half-wave plate, then was reflected by an SLM (Hamamatsu X10468-02) with 10° angle of incidence. A hybrid hologram loaded on the SLM was generated by a binary grating and an expected geometric mask. After the SLM, the laser beam was split into diffractive beams and the 0 order beam. A slit was placed behind the Lens 1 to block the diffractive beams. Two positive lenses (focal length: f_1=1000mm, f_2=30mm) formed a *4f* imaging system, and the demagnification of the beam was around 33X. A polished stainless steel sample were mounted on a three-axis motion control system (Aerotech) at the image plane. A pick-off (1%) beam splitting mirror, placed after the slit, diverted the beam through the Lens 3 (focal length: f_1=1000mm) which formed another *4f* imaging system with the Lens 1. A CCD camera (Spiricon) was placed at Plane A″ to observe the reconstructed beam shape.

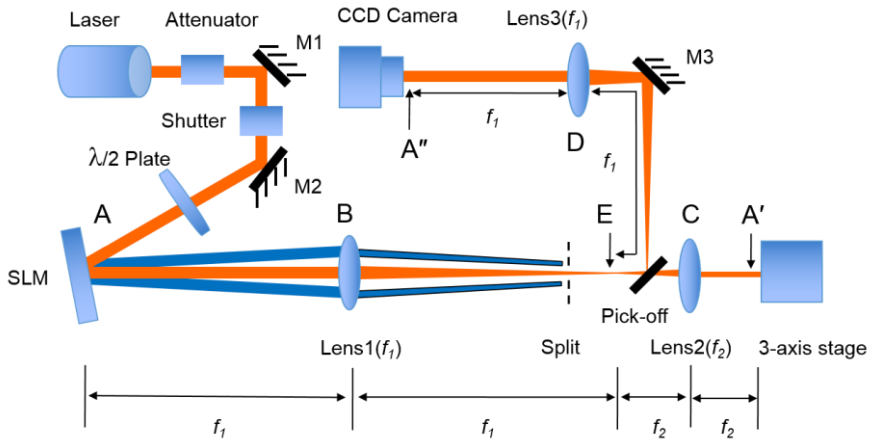

Fig. 1.Experimental setup.

2.2 Beam shaping using hybrid holograms

Fig. 2 shows the principle of beam shaping using a hybrid hologram combined by the binary grating and a geometric mask. The SLM (Hamamatsu X10468-02) was a phase-only parallel-aligned nematic liquid crystal device and could achieve a π phase modulate when the gray level was 105. The binary grating composed by two different gray levels, was designed to produce a π phase shift. Therefore, the two gray level of the binary grating were set to G_1=0, G_2=105. The geometric mask with a desired shape were set to zero gray level, which produce zero phase delay and act as a mirror.

The incident light polarization was set to horizontal. After the laser beam reflected of the SLM, it was diffracted into several beams and the energy was mainly distributed into ±1st order and 0 order, as shown in Fig. 2. The ±1st order beams were blocked by a slit.

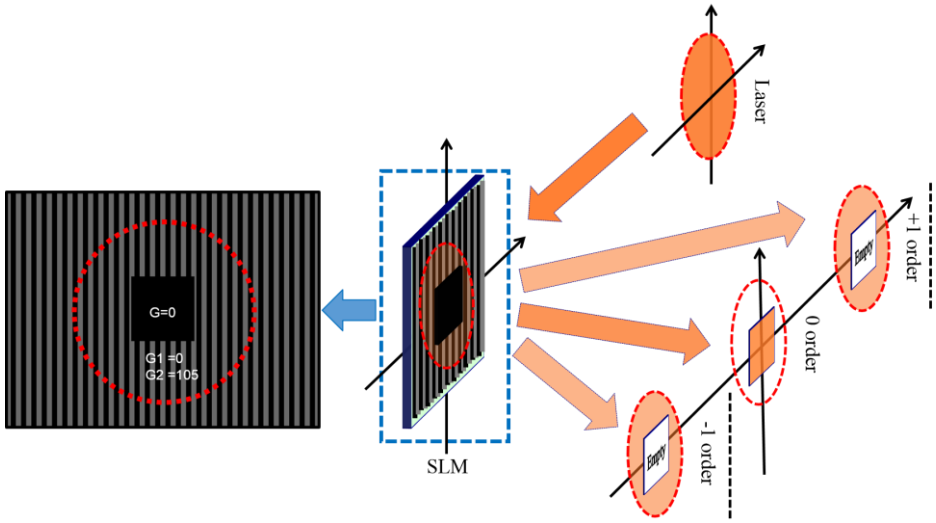

Fig. 2. The principle of beam shaping using a hologram combined by a binary grating and a geometric mask

2.3 Intensity distribution of the shaped beam after SLM

The relationship between the amplitude of a Gaussian beam and the beam radius r is:

$$A = A_0 e^{-\frac{r^2}{\omega^2}}, \tag{1}$$

Where A_0 is the amplitude of the center of the beam section. The diffraction efficiency of the step approximation to the binary grating can be obtained by expanding its periodic amplitude transmittance in a Fourier series. A calculation shows that the diffraction efficiency of the m diffraction order can be expressed by [17]

$$\eta_m = \sin c^2\left(\frac{m}{2}\right)\frac{\sin c^2(m-1)}{\sin c^2\left(\frac{m-1}{2}\right)}, \tag{2}$$

According to equation (2), the diffraction efficiency of ± 1st order is 40.5%, and the zero order is 0. Thus, the intensity distribution of the shaped beam after the SLM is

$$I_{shaped} = A^2 \quad S \le S_{mask}, \tag{3}$$

Where S_{mask} is the area of the mask. Figure 1 shows the corresponding area of the mask and the incident beam after loading the hybrid hologram on the SLM. The shaping efficiency η_{shaped} is determined by

$$\eta_{shaped} = \frac{\iint I_{shaped} ds_{mask}}{\iint I_{incident} ds_{incident}}, \tag{4}$$

Where $\iint I_{shaped} ds_{mask}$ is the integral of the shaped area intensity profile and $\iint I_{incident} ds_{incident}$ is the integral of the incident beam intensity profile. Equation 4 can be simplified as follows:

$$\eta_{shaped} = \frac{\iint A^2 ds_{mask}}{\iint A^2 ds_{incident}}, \tag{5}$$

Therefore, the shaping efficiency of the beam is theoretically related to the area of the mask, that is, the area of the shaping beam. However, due to the loss on the SLM, the actual ± 1st order diffraction efficiency of the binary grating is lower than the theoretical value of 40.5%, which leads to the addition of the extra beam energy to the 0 order beam, resulting in the change of the shaping efficiency and the quality of the shaped beam.

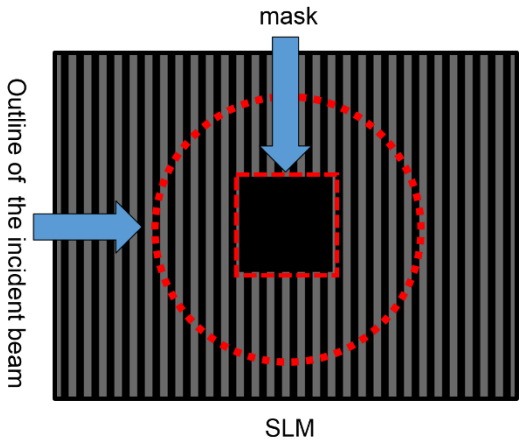

Fig. 3. The relative position of the hologram and the incident beam on the SLM

In this case, the binary grating period Λ affects the diffraction angle and the diffraction efficiency. The diffracted beams corresponding to consecutive orders may overlap which influence the quality of the shaped beam. Therefore, the optimal grating period should be determined. The diffraction angle β can be calculated based on the following grating equation:

$$\Lambda(\sin\alpha + \sin\beta) = m\lambda\,, \tag{6}$$

where α is the incident angle, m is the diffraction order and λ is the wavelength of the input light. The +1st order diffraction angle β can be expressed as:

$$\beta \approx \sin\beta = \lambda/\Lambda - \sin\alpha\,, \tag{7}$$

In the experimental setup, $\sin\alpha$ (α < 10°) is very small and can be neglected, then equation (7) can be rewritten as

$$\beta = \lambda/\Lambda\,, \tag{8}$$

From equation (8), it can find that β and grating period Λ have an inverse relationship. For avoiding the overlap between the 0 order beam and ±1st order beams, it should increase the diffraction angle β through reducing the grating period Λ. However, as the period decreases, the diffraction efficiency of the grating will be reduced[18], which may lead to the 0 order optical energy of the non-masked region is higher than

the material damage threshold. Therefore, the selection of the optimal grating period has to consider both diffraction angle and diffraction efficiency.

3. Results and discussion

3.1 Grating period

In order to obtain a uniform energy distribution in the central area, the geometry mask size was set to 2 × 2 mm^2, which was the same size as the image detected in the CCD camera. In order to evaluate the influence of the grating period Λ on the shaped beam, experiments with different periods based on the same square mask were carried out. Fig. 4 shows the beam shaping results of observing at CCD camera (A″) and the ablation on the polished stainless steel sample with Λ=160 μm, 320 μm, 400 μm and 500 μm. The incident pulse energy E_p on the SLM was approximately 25 μJ, and the exposure time was 0.5 s (5000 pulses).

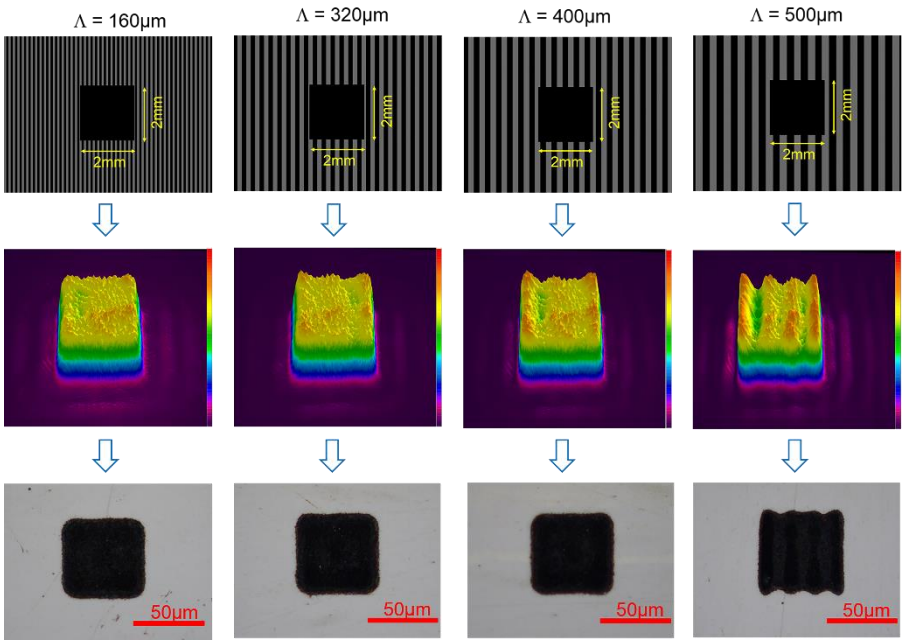

Fig. 4. The beam profiles observed at CCD camera (A″) and the ablation with Λ=160μm, 320μm, 400μm and 500μm.

When Λ=160 μm, the square beam is of high quality, shown by the extremely low background scatter and uniform top-hat profile. When the grating period Λ increases, partial ±1st order beam, which is not blocked by the slit, overlaps with the 0 order beam and causes interference, as shown in Fig. 4.

3.2 Local energy ratio

In order to quantitatively analyze the effect of the grating period on the quality of the shaped beam, the concept of local energy ratio ξ is introduced, which is defined as [19]:

$$\xi = \frac{\iint I_{shaped} ds_{mask}}{\iint I_0 ds}. \tag{9}$$

where $\iint I_0 ds$ is the integral of the original beam intensity profile obtained at A″. It represents the beam quality, and the higher the local energy ratio, the better the beam quality. As shown in Fig. 5, when the grating period changes from 120 μm to 500 μm, the local energy ratio is varied from 72% to 85%. It means that there is a very obvious boundary between the shaped area and the non-shaped area in the current region. And it is much higher than that of the previously method obtained by adjusting the amplitude of the incident beam, which is only about 30% when the incident beam is 2 mm [19]. When the grating period is higher than 320μm, the efficiency remains essentially unchanged, which is due to the high-order beam is not completely separated affecting the overall efficiency. Compared with 160μm and 320μm periods, the local energy ratio of the former is 7% lower than that of the latter, but the distance between +1st order beam and 0 order beam is twice of the latter. Considering the influences of diffraction angle and local energy ratio, the smaller period Λ = 160 μm is selected. Then the distance between +1st order beam and 0 order beam at the slit is 5 mm and the local energy ratio is up to 77.67%.

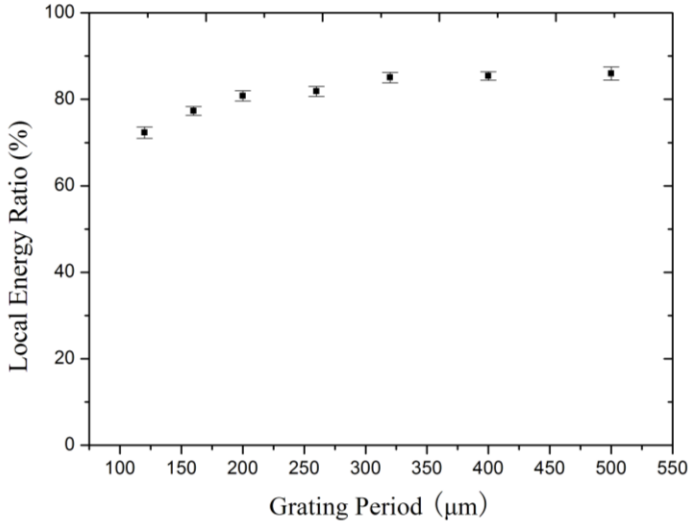

Fig. 5. The variation of the local energy ratio of the shaping beam observed at A″ by the CCD camera when changing the grating period.

3.3 The reconstructed range of shaped beam

Because of the spherical aberration caused by the focal length difference between the lens 1 and the lens 2 (focal length: f_1=1000mm, f_2=30mm), the shaping beam can′t always maintain the shaped profile after the lens 2. In order to measure the reconstructed distance of shaping beam, the experiments with squared top-hat beam machined on a polished stainless steel sample are carried out. The ablation patterns were produced at difference positions close to the image plane A′. As shown in Fig. 6, the spot at the plane of Δ= +0.3 mm is not the desired shape, accompanied by deformation. As the distance decreases, the beam shape is successfully reproduced with a size of 55μm, but at the plane of Δ= -0.4 mm again deformed. This indicates that the desired profiles can be reconstructed within a range of 0.5 mm (Δ= +0.2 mm ~Δ= -0.3 mm) around the imaging plane A′.

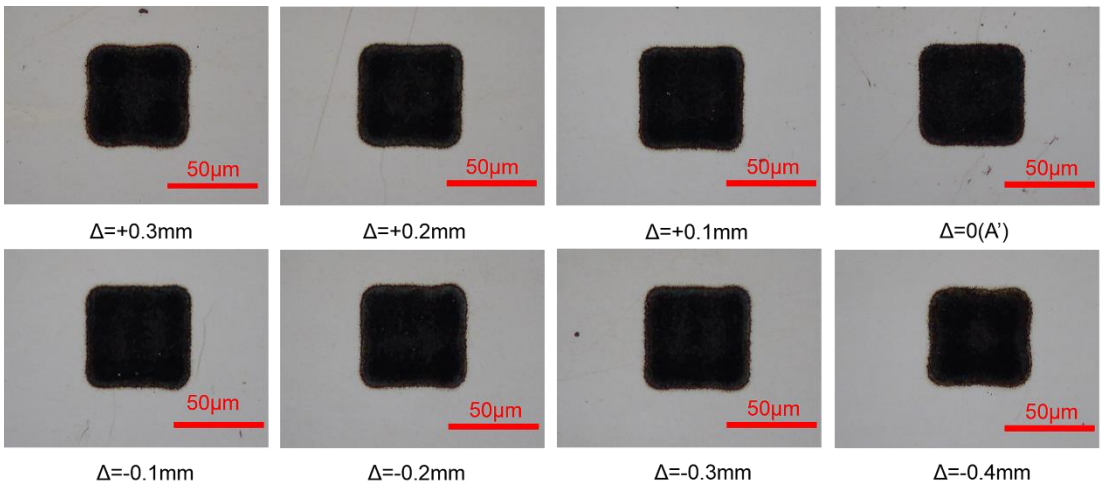

Fig. 6. The results of the squared flattop beam machined at difference distance to the image plane A′. Δ=0 denote it is on Plane A'.

3.4 Dynamic transformation of high quality shaped beams

As shown in Fig. 7, by loading different hybrid holograms onto the SLM, the CCD camera at the plane of A″ can observe the spot is shaping into a ring, triangle, pentagon and hexagon. While at Plane A′, corresponding ablation patterns can also be achieved.

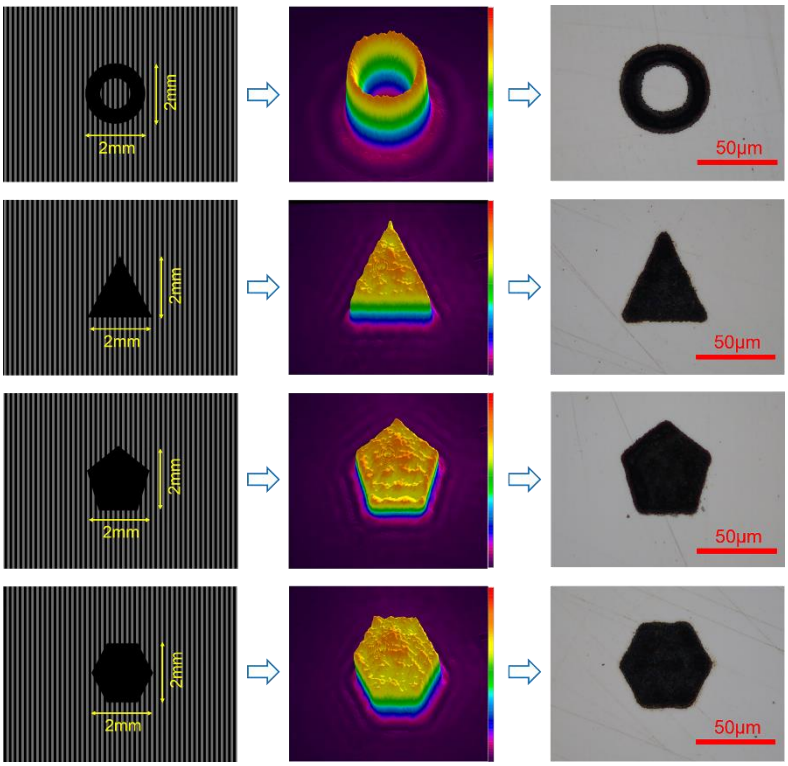

Fig. 7. Different shapes can be observed on the CCD camera and also on the polished stainless steel surface.

Fig. 8 shows the results of beam shaping with the hybrid holograms and simple apertures. The SLM were replaced with physical apertures with different shapes, such as triangular, pentagonal and hexagonal. The beams shaped using apertures have severe edge diffraction effects. While, the beams produced with the hybrid holograms can effectively reduce such effects and present uniform flattop intensity profiles.

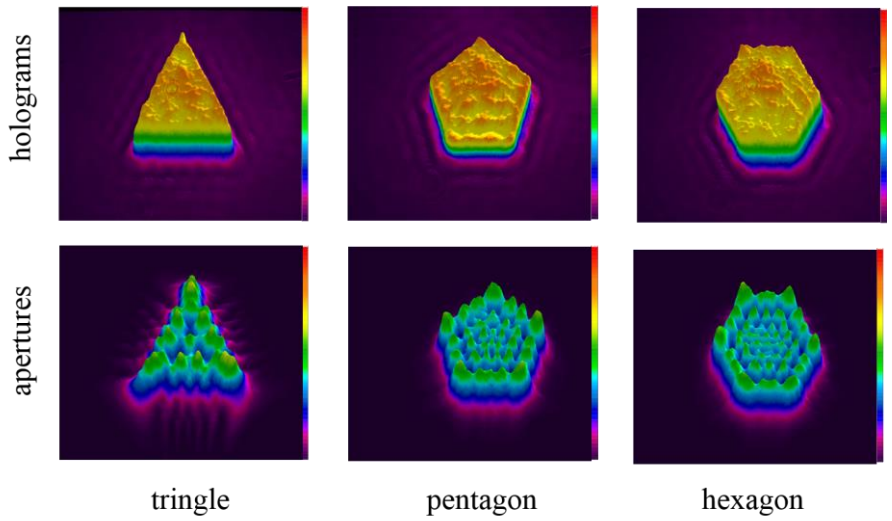

Fig. 8. Beam shaping with the hybrid holograms and apertures

Fig. 9 depicts the ablation on the polished stainless steel surface by displaying 4 holograms in sequence. The input pulse energy E_p on the SLM is 40 μJ. Due to the inherent slow refresh rate of the liquid crystal device, the dynamic machining rate was limited to 25 Hz. Much higher dynamic machining rate can be achieved, if a high speed MEMS type of SLM is employed.

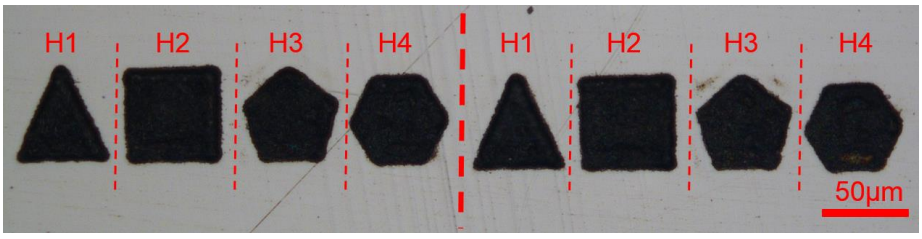

Fig. 9. The ablation traces of the shaping beam machined on the polished stainless steel surface at 25Hz dynamic refresh rate of 4 holograms and 40μJ incident pulse energy.

4. Conclusions

Laser beam shaping with hybrid holograms is a novel method to improve the quality of shaped beams. The edge diffraction effect has been significantly reduced. Top-hat beam with arbitrary profile can be easily obtained in the diffraction near-field

by changing the simple hybrid holograms, and the shaped beam can be reconstructed in a range of 0.5 mm at the image plane. The ablation on the polished stainless steel sample by the reconstructive beam profile are consistent with the beam shapes observed on the CCD camera. The grating period affects the shaped beam quality and the diffraction efficiency. The +1st order beam that affects the shaped beam can be completely removed when the grating period is 160μm, while the local energy ratio of the shaped beam observed at by the CCD camera is up to 77.67%. And dynamic machining at 25 Hz with different shapes has also been achieved.

5. Acknowledgments

The authors gratefully acknowledge the support of the National Natural Science Foundation of China (51575164, 51405143), National Key Technology Research and Development Program of the Ministry of Science and Technology of China (2015BAF20B03), and Science and Technology support program of Hubei province (2015BAA066).

Reference

[1] C. Mauclair, D. Pietroy, Y. Di Maïo, E. Baubeau, J.-P. Colombier, R. Stoian, F. Pigeon, Ultrafast laser micro-cutting of stainless steel and PZT using a modulated line of multiple foci formed by spatial beam shaping, Opt. Lasers Eng. 67 (2015) 212–217.

[2] D.S. Qian, X.L. Zhong, Y.Z. Yan, T. Hashimoto, Z. Liu, Microstructures induced by excimer laser surface melting of the SiC p /Al metal matrix composite, Appl. Surf. Sci. 412 (2017) 436–446.

[3] Z.W. Xue, Y.D. Guo, Z.Z. Chen, S. Li, Y.T. Xu, J. Xu, B.S. Wang, K.L. Gong, H.W. Gao, Y. Bo, Q.J. Peng, D.F. Cui, Z.Y. Xu, Actively compensation of low order aberrations by refractive shaping system for high power slab lasers, Opt. Laser Technol. 75 (2015) 71–75.

[4] M. Duocastella, C.B. Arnold, Bessel and annular beams for materials processing, Laser Photon. Rev. 6 (2012) 607–621.

[5] L. Yang, A. El-Tamer, U. Hinze, J.W. Li, Y.L. Hu, W.H. Huang, J.R. Chu, B.N. Chichkoy, Parallel direct laser writing of micro-optical and photonic structures using spatial light modulator, Opt. Lasers Eng. 70 (2015) 26–32.

[6] K. Dev, A. Asundi, Polarization modulation study of transmissive liquid crystal spatial light modulator using digital holographic polariscope, Opt. Laser Technol. 47 (2013) 323–328.

[7] A. Shibukawa, A. Okamoto, M. Takabayashi, A. Tomita, Spatial cross

modulation method using a random diffuser and phase-only spatial light modulator for constructing arbitrary complex fields, Opt. Express. 22 (2014) 3968.

[8] Y. Nie, X. Li, J. Qi, H. Ma, J. Liao, J. Yang, W. Hu, Hollow Gaussian beam generated by beam shaping with phase-only liquid crystal spatial light modulator, Opt. Laser Technol. 44 (2012) 384–389.

[9] N. Védrenne, L.M. Mugnier, V. Michau, M.-T. Velluet, R. Bierent, Laser beam complex amplitude measurement by phase diversity, Opt. Express. 22 (2014) 4575–4589.

[10] S.S. Li, Y.L. Wang, Z.W. Lu, L. Ding, C. Cui, Y. Chen, P.Y. Du, D.X. Ba, Z.X. Zheng, H. Yuan, L. Shi, Z.X. Bai, Z.H. Liu, C.Y. Zhu, Y.K. Dong, L.X. Zhou, Spatial beam shaping for high-power frequency tripling lasers based on a liquid crystal spatial light modulator, Opt. Commun. 367 (2016) 181–185.

[11] H. Kim, C.-Y. Hwang, K.-S. Kim, J. Roh, W. Moon, S. Kim, B.-R. Lee, S. Oh, J. Hahn, Anamorphic optical transformation of an amplitude spatial light modulator to a complex spatial light modulator with square pixels [invited]., Appl. Opt. 53 (2014) G139-46.

[12] J. Li, Z. Kuang, S. Edwardson, W. Perrie, D. Liu, G. Dearden, Imaging-based amplitude laser beam shaping for material processing by 2D reflectivity tuning of a spatial light modulator, Appl. Opt. 55 (2016) 1095–1100.

[13] S.W. Bahk, E. Fess, B.E. Kruschwitz, J.D. Zuegel, A high-resolution, adaptive beam-shaping system for high-power lasers, Opt. Express. 18 (2010) 9151.

[14] P.W.M. Tsang, a. S.M. Jiao, T.-C. Poon, Fast conversion of digital Fresnel hologram to phase-only hologram based on localized error diffusion and redistribution, Opt. Express. 22 (2014) 5060.

[15] D. Wang, J. Zhang, H. Wang, Y. Xia, Variable shape or variable diameter flattop beam tailored by using an adaptive weight FFT-based iterative algorithm and a phase-only liquid crystal spatial light modulator, Opt. Commun. 285 (2012) 5044–5050.

[16] A. Forbes, A. Dudley, M. McLaren, Creation and detection of optical modes with spatial light modulators, Adv. Opt. Photonics. 8 (2016) 200.

[17] E. Huggins, Introduction to Fourier Optics, McGraw-Hill, Inc., 1976.

[18] K. Chaen, H. Takahashi, S. Hasegawa, Y. Hayasaki, Display method with compensation of the spatial frequency response of a liquid crystal spatial light modulator for holographic femtosecond laser processing, Opt. Commun. 280 (2007) 165–172.

[19] Z. Kuang, J. Li, S. Edwardson, W. Perrie, D. Liu, G. Dearden, Ultrafast laser beam shaping for material processing at imaging plane by geometric masks using a spatial light modulator, Opt. Lasers Eng. 70 (2015) 1–5.